Cellulose (2022) 29:3859–3870
https://doi.org/10.1007/s10570-021-04327-2

ORIGINAL RESEARCH

# Exploiting chitosan to improve the interface of nanocellulose reinforced polymer composites

**Meghan E. Lamm · Kai Li · Darby Ker · Xianhui Zhao · H. E. Hinton · Katie Copenhaver · Halil Tekinalp · Soydan Ozcan**

Received: 11 August 2021 / Accepted: 8 November 2021 / Published online: 22 March 2022


**Abstract** Cellulose nanofibrils (CNFs) have been widely used as a nanofiller for polymer composite reinforcement due to their excellent mechanical properties. However, CNF is produced in water and needs to be dried prior to use in composite materials. The presence of hydroxyl groups on the surface of CNF creates strong hydrogen bonding that makes it difficult and costly to dry. Additionally, the hydrophilicity at the fiber surface results in agglomeration of CNFs within many polymer matrices. In this study, chitosan (CS) was co-precipitated with CNF to produce a dual-bonding filler for use in poly (lactic acid) (PLA) composites. CS promotes improved interfacial interaction within the polymer matrix by forming strong hydrogen bonds with the CNF and potential covalent bonds with the PLA. The results confirmed that the addition of a small amount of CS significantly improved the mechanical properties compared to PLA + CNF composites and neat PLA. The detailed study of the PLA + CNF/CS composites reveals the synergetic effect of the hydrogen and covalent bonding mechanism for PLA reinforcement.

**Supplementary Information** The online version contains supplementary material available at https://doi.org/10.1007/s10570-021-04327-2.

M. E. Lamm · X. Zhao · K. Copenhaver · H. Tekinalp · S. Ozcan (✉)
Oak Ridge National Laboratory, Manufacturing Science Division, 1 Bethel Valley Road, Oak Ridge, TN 37831, USA
e-mail: ozcans@ornl.gov

K. Li (✉)
Oak Ridge National Laboratory, Buildings and Transportation Science Division, 1 Bethel Valley Road, Oak Ridge, TN 37831, USA
e-mail: lik1@ornl.gov

D. Ker · H. E. Hinton
Oak Ridge National Laboratory, Chemical Sciences Division, 1 Bethel Valley Road, Oak Ridge, TN 37831, USA

**Graphical abstract**

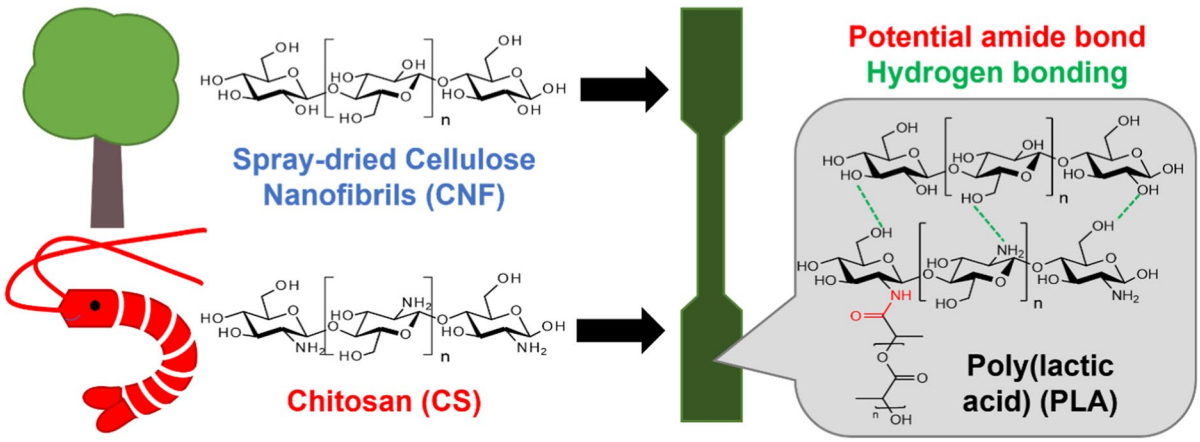


**Keywords** Cellulose nanofibrils (CNF) · Chitosan (CS) · Poly (lactic acid) (PLA) · Composites · Interfacial engineering

## Introduction

Nanocellulose has gained traction in the research community due to its use across a range of scientific fields (Abitbol et al. 2016; Isogai 2020; Lamm et al. 2021; Li et al. 2021a). One specific type of nanocellulose, cellulose nanofibrils (CNFs), are being used as reinforcement fillers in a range of composite materials due to their high specific strength and stiffness (Jawaid et al. 2017; Li et al. 2021b; Meng et al. 2018; Tekinalp et al. 2019; Wang et al. 2020, 2018b). CNFs can be derived from various plants, algae, and other biological materials, which makes them a green, sustainable alternative to the glass and carbon fibers derived from non-renewable materials that are traditionally used in composites (Abdul Khalil et al. 2012) CNFs are comprised of both individuals and bundles of nanoscale fibrils of polymeric repeating β-(1–4 linked), D-glucose linkages, held together tightly through hydrogen-bonding of the surface hydroxyl groups. Most CNF is produced using water-based fibrillation methods, which serves to mechanically pull apart larger bundles into this nanoscale material (Nechyporchuk et al. 2016). Unfortunately, strong hydrogen-bonding between water and CNF, and among CNFs lead to a tightly bounded CNF structure during the water removal process (drying). During the drying process, hydroxyl groups on the surface of the CNF form strong hydrogen-bonds through a process called hornification (Beaumont et al. 2017). This results in irreversible agglomeration, producing a CNF material incapable of dispersion within a polymer matrix. Hornification is common during oven and air-drying techniques.

In order to incorporate CNFs into composites through industrially viable processes, e.g., extrusion, water needs to be removed to prevent degradation of the polymer matrix, especially when used in biopolymers, and formation of porosity. A few strategies exist to dry CNF without the occurrence of hornification, but many, including freeze-drying and supercritical $CO_2$ drying, remain costly and difficult to use industrially (Peng et al. 2012; Sinquefield et al. 2020; Zimmermann et al. 2016). Additionally, CNFs, which are hydrophilic in nature, tend to aggregate when introduced into polymer matrices, as most are hydrophobic (Zhou et al. 2016). In order to achieve good mechanical properties in a composite material, the filler must remain homogeneously dispersed throughout the matrix. Many researchers have turned to surface modification to reduce CNF agglomeration and aid in the drying process, as these modifications can decrease the surface energy, disturb hydrogen-bonding, and prevent hornification (Habibi 2014;

Kalia et al. 2013; Missoum et al. 2013; Rol et al. 2019). CNF surface modifications can be classified under three major strategies: adsorption, molecular grafting, and polymer grafting. Strategies that involve the formation of covalent bonds, including molecular and polymer grafting, are stronger, more stable, and tend to support greater mechanical enhancement than adsorption. Wang et al. used maleic anhydride as a coupling agent to form a reinforced interface in polypropylene/CNF composites (Wang et al. 2018a). The mechanical properties improved due to the presence of covalent bonds at the interface which served to adequately disperse stress. Surface modifications, such as adsorption, relying solely on molecular interactions among filler or between filler and matrix, like hydrogen bonding, must be tailored in order to prevent formation of a weak phase or matrix plasticization in thermoplastic composites (Bréchet et al. 2001). However, research has shown that proper exploitation of molecular interactions can produce strong interfaces through interfacial engineering. For example, an extensive research has found that poly(vinyl alcohol) (PVOH)/CNF composites form extremely strong hydrogen bonds between the hydroxyl groups on both the PVOH side chains and CNFs, resulting in mechanically robust composites (Liu et al. 2013; Peng et al. 2014; Peresin et al. 2010). Other researchers have also successfully exploited these interactions to produce a range of materials featuring strong, reversible crosslinking through hydrogen bonds, which have seen use in a host of applications including self-healing materials (An et al. 2019; Hu et al. 2015; Lamm et al. 2019).

Chitosan (CS) is a biopolymer that can be isolated from crustaceans. It is comprised of β-linked D-glucosamine and N-acetyl-D-glucosamine units and features primary amine and hydroxyl groups which can form interactions with other molecules.(Bakshi et al. 2020) Traditionally, CS is used in composites specifically for biomedical and packaging applications, as such, their tensile mechanical properties are often not fully characterized.(Rinaudo, 2006) CS is a poor reinforcing agent by itself in composites for high performance applications due to its inferior mechanical properties, but it can be combined with other bio-based fillers such as CNF to achieve superior performance (Abdul Khalil et al. 2016) A few researchers have exploited this strategy for applications such as reinforced composites for packaging and antibacterial textiles (Ali Raza et al. 2019; Niu et al. 2018). Rizal et. al. utilized a high loading of CS as a comatrix for CNF filled biodegradable PLA composites (Rizal et al. 2021). The fibrous morphology of the CNF, obtained using supercritical $CO_2$ drying, produced good reinforcement.

In this study, a dual-bonding strategy is introduced using a CS coating on the surface of CNF to strengthen the interface between PLA/CNF composites. PLA is a mechanically robust, bio-based polymer that can serve as a competitive replacement for petroleum-based polymers, such as acrylonitrile–butadiene–styrene (ABS), in composite materials. Li et al. has shown that CS can be exploited in a dual-bonding strategy to form a strong interface in CNF films (Li et al. 2019). Additionally, Zhao et al. and Lu et al. demonstrated that the incorporation of pendant amine groups ($–NH_2$) can result in amide formation after compounding with polylactic acid (PLA), which contains carboxylic acid (–COOH) polymer chain ends (Lu et al. 2015; Zhao et al. 2020). Similarly, Shah et al. used CS to improve the interface between a wood flour/PLA composite (Shah et al. 2008). The addition of CS was suspected to form an amide bond with PLA, however the low loading levels of CS used and presence of residual amides on the CS made it difficult to confirm. It is hypothesized that the CS surface modification on CNF can facilitate synergistic effects between a combination of hydrogen bonding and theoretical covalent bonding in PLA composites. This can be accomplished through two bonds; covalent amide bonds between pendant amide groups on CS and the acid chain ends of PLA, and extensive hydrogen bonding formed between the hydroxyls chain ends of PLA and pendant hydroxyl groups on both CNF and CS. Spray dried CNF was chosen for modification as it is a commercially available CNF source but struggles to maintain mechanical properties at higher loadings (> 10 wt%) due to its low aspect ratio. Exploiting this commercial material to produce a range of high-performance composites can thrust the use of CNF composites into large-scale markets such as manufacturing. First, the level of CS functionalization was tailored to produce an adequate interface, determined to be 2.5 wt% CS on the CNF surface (CNF/2.5CS). The CNF/2.5CS were then dispersed in a PLA matrix to obtain composites. Compared with literature, our modified spray dried CNFs maintain tensile strength and display an increase

in Young's modulus with increasing fiber content, which is currently unseen in the literature for spray dried materials. Extensive characterization, including thermal and morphological analyses, showed that this potential dual-bonding strategy was successfully utilized to achieve well-dispersed nanocomposites with significantly enhanced mechanical properties.

## Experimental

### Materials

Spray dried bleached cellulose nanofibril (90% fine) was obtained from the University of Maine. Poly(L-lactide) Ingeo 4043D (referred to as PLA or PLA4043D in this work) with 94% L-lactic acid content, a number average molecular weight ($M_n$) of 67 kDa and dispersity (Đ) of 2.2 (measured by gel permeation chromatography (GPC)) was purchased from NatureWorks LLC (Minnetonka, Minnesota). Chitosan (CS, 75–85% degree of deacetylation, medium molecular weight), and sodium hydroxide (NaOH) were purchased from Sigma-Aldrich (St. Louis, MO, USA).

#### *CNF/CS preparation*

CNF/CSs were prepared using a co-precipitation method. Briefly, 5 g of spray dried CNF was redispersed in DI water under vigorous stirring. Desired amount of the CS solution (5 mg/mL in 2 v/v % acetic acid) was added to CNF suspension. Then, the mixture was neutralized with NaOH (1 M). The resultant suspension was filtered and dried at 80 °C in an oven till constant weight. CNF/CS with CS content of 2.5, 5, 7.5, 10, and 20 wt% were prepared (Table 1).

**Table 1** CNF/CS samples prepared with varying CS content

| Sample Name | CS Content (wt%) |
|---|---|
| CNF/2.5CS | 2.5 |
| CNF/5CS | 5 |
| CNF/7.5CS | 7.5 |
| CNF/10CS | 10 |
| CNF/20CS | 20 |

#### *Composite sample preparation*

All materials were dried at 80 °C in a convection oven for 4 h before compounding to remove any moisture in the sample. PLA + CNF/2.5CS composites were prepared in a melt mixer (Intelli-Torque Plasti-Corder half-size mixer, C. W. Brabender, Instruments Inc.) by initially melting PLA at 175 °C for 3 min at 60 rpm and then adding the desired amount of CNF/2.5CS slowly into the PLA melt and shear mixing for another 5 min. Neat PLA, PLA + CNF, and PLA + CS composites were prepared using the same procedure. The content of CNF/2.5CS and CNF ranged from 5 to 30 wt%. Additional samples were compounded using PLA and 5 wt% fiber content of higher CS loaded CNF (CNF/5CS and CNF/7.5CS). After compounding, the mixtures were hot pressed into 1 mm films at 180 °C. The thin films were then cut into slices and then compression molded into uniform bars at 180 °C following ASTM standard D4703 and further cut into dog-bone specimens (ASTM D638 type-V).

### Methods

#### *Characterizations*

*Tensile Testing:* Tensile properties was measured by stretching the dog-bone specimens at room temperature via a servo-hydraulic testing machine with a 2000 N loading cell at a speed of 1.5 mm/min. Four specimens for each sample were tested and the average was reported.

*Scanning electron microscopy (SEM)* The cross section of films was sputtered with iridium and imaged with a Zeiss Merlin VP SEM/scanning transmission electron microscope system at a low voltage of 1 kV.

*Attenuated total reflectance infrared spectroscopy (ATR-IR)* ATR-IR absorption spectra of the films were measured with a Thermo Nicolet Nexus 670 Fourier transform infrared spectrometer with a diamond ATR attachment with a spectral resolution of 2 $cm^{-1}$ in the range of 4000–600 $cm^{-1}$.

*X-ray photoelectron spectroscopy (XPS)* XPS was performed with a Thermo Scientific Model K-Alpha

XPS instrument, which was equipped with micro-focused, monochromatic Al Kα x-rays (1486.6 eV) that were focused to a range of spot sizes from 30 to 400 microns. Wide energy range survey spectra (0–1350 eV) were acquired for qualitative and quantitative analysis (pass energy = 200 eV; step size = 1.0 eV). Assessment of chemical bonding of the identified elements was accomplished by collecting core-level spectra over a narrow energy range (pass energy = 50 eV; step size = 0.1 eV). Data were collected and processed using the Thermo Scientific Avantage XPS software package (v. 4.61). When necessary, spectra were charge corrected using the C 1 s core-level peak set to 284.6 eV.

*Solid state NMR (CP MAS $^{13}C$ SS-NMR) spectroscopy* Solid-state NMR experiments were performed on a Bruker Avance-III 400-MHz (9.4 Tesla) spectrometer (Bruker Biospin Corporation, Bellerica, MA, USA) operating at Larmor frequencies of 100.63 MHz for $^{13}C$ nucleus using a 4-mm double-resonance magic angle spinning (MAS) probe head. The samples were packed into a 4-mm cylindrical zirconia dioxide MAS rotor. The experiments were conducted at room temperature (296 k) at MAS frequencies of 8 kHz. $^{1}H$-$^{13}C$ cross-polarization (CP) with ramped (70–100%) $^{1}H$ rf amplitude and 1.5 ms contact pulse was used to obtain the initial transverse magnetization for CP/MAS experiments. The radiofrequency field strength was 55.5 kHz for $^{1}H$ and $^{13}C$ in the CP pulse. High power proton decoupling (SPINAL-64) was applied during acquisition at a $^{1}H$ nutation frequency of 70 kHz. A 4 s recycle delay and 1500 – 2048 scans were used. The $^{13}C$ chemical shifts were calibrated by externally referencing to methylene signal of adamantane at 38.48 ppm on the tetramethylsilane scale. The cellulose crystallinity index (CrI) was determined from the integration areas of the crystalline and amorphous C-4 signals of CP/MAS $^{13}C$ NMR spectra using Eq. 1:

$$CrI = \frac{A_{86-92\text{ppm}}}{A_{79-86\text{ppm}} + A_{86-92\text{ppm}}} \times 100 \quad (1)$$

where $A_{86\text{-}92\ \text{ppm}}$ and $A_{79\text{-}86\ \text{ppm}}$ are the areas of the crystalline and amorphous C4 carbon signals of cellulose, respectively.

*Thermogravimetric Analysis (TGA):* The degradation temperatures were determined by thermogravimetric analysis (TGA) using a TA Instruments Q500 apparatus. The samples were heated from room temperature at 10 °C/min to 600 °C.

*Inverse gas chromatography (iGC)* The dispersion component of surface energy and acid–base characteristics of samples were measured and calculated based on a SMS-iGC device (Surface Measurement Systems, London, UK). Detailed mechanism and description of this methodology can be found in previous work (Peng et al. 2013). A pre-silanized glass tube, 30 cm in length and 4 mm in inner diameter was used. CNF powders were introduced into the tube by a hopper and an electric vibrator to fill 2/3 of the total tube volume. After the sample was added into the tube, the other end of the glass tube was plugged with silanized glass wool. Once the glass tube was in place, helium was used as the carrier gas and methane was used as a reference gas. Conditions for running the test were 0% of RH and 10 standard cubic centimeters per minute (sccm) of carrier gas flow rate. Before running a test, columns were conditioned in situ for 4 h at 30 °C. The detection method of retention times of the probe gases was determined using a flame ionization detector. Analysis was completed using the Cirrus SEA control software. The peak maximum method was used to determine the retention time of all probe gases (Conder and Young 1979). The dispersion component of surface energy and acid–base characteristics were calculated (Fowkes 1964; Gutmann 1978; Schultz et al. 1987).

*Dynamic mechanical analysis (DMA)* DMA of the composite was carried out using the TA Instruments DMA Q800 in multi-frequency—strain mode with a dual cantilever clamp. The measurements were performed at a constant frequency of 1 Hz with a temperature range from room temperature to 120 °C at a heating rate of 3 °C/min. The test specimen dimensions were about 3 mm × 10 mm × 63 mm (thickness × width × length).

*Differential scanning calorimetry (DSC)* DSC was performed on a TA Instruments Q2000 apparatus using heat/cool/heat mode. The scanning conditions were set as follows: each sample was equilibrated at 25 °C and then heated to 200 °C at 10 °C $min^{-1}$. The sample was then cooled at 10 °C $min^{-1}$ to 25 °C. During the second heating cycle the sample was heated to 200 °C at 10 °C $min^{-1}$. The degree of crystalliza-

tion ($\chi c$) was derived from Eq. 2 using first-heat curve, where $\Delta H_m$ and $\Delta H_c$ are the melting and crystallization enthalpies of the nanocomposite. $\Delta H_{100}$ and $w$ are the melting enthalpy for 100% crystalline PLA and weight fraction of PLA in the composite. The $\Delta H_{100}$ value used for the calculation was 93 J/g (Fujisawa et al. 2013).

$$\chi_c = \frac{\Delta H_m - \Delta H_c}{\mathrm{w} \times \Delta H_{100}} \quad (2)$$

## Results and discussion

### CNF/CS synthesis and characterization

CS-coated CNF (CNF/CS) was produced using a coprecipitation strategy (Scheme 1) and contained an overall content of CS varying from 2.5 to 7.5 wt% with respect to the CNF. To produce the materials, CS was dissolved in a dilute acetic acid solution (2 v/v %) and combined with a spray dried CNF dispersion in water. Sodium hydroxide (NaOH) was then added dropwise to precipitate the CS and entwine it around the surface of the CNF. Due to its high molecular weight and pH-responsive amine groups, CS becomes water-insoluble at pH > 5–6. This behavior has been exploited by researchers to produce encapsulated or coated materials, and one common application uses CS coprecipitated with $Fe_3O_4$ for magnetic absorbents (Cai et al. 2018; Pu et al. 2018).

Extensive characterization was performed to confirm the presence of CS on the surface of CNF and success of our coprecipitation methodology. X-ray photon spectroscopy (XPS) was used to analyze the surface of the functionalized CNF (Fig. 1a). Most of the spectra appeared similar to the neat CNF, with C 1 s peaks between 284–290 eV and an O 1 s peak around 533 eV. There was one peak unique to CS around 339.7 eV, consistent with the N 1 s level of CS. Likewise, Fourier-transform infrared spectroscopy (FTIR) indicated presence of CS on the CNF surface, confirmed via the presence of a peak at 1565 $cm^{-1}$, consistent with N–H bending (Fig. 1b). The peak in the Fig. 1b is weak; however, when the CS loading is increased to 10 wt% or above, a clear peak of N–H bending is visible as shown in Fig. S4A. Thermal degradation was measured using thermal gravimetric analysis (TGA, Fig. 1c). The presence of CS on the surface of CNF affected the degradation behavior, increasing the initial degradation temperature slightly (294–303 °C) and causing a significant decrease in char yield (~ 20 to < 5%).

The morphology of the functionalized CNF was examined using scanning electron microscopy (SEM), which confirmed that the particle shape and size did not change after CS functionalization (Fig. 1d–g and S1). However, the CNF/CS particles became smoother compared to the CNFs before functionalization, suggesting the presence of the CS. The overall surface chemistry was analyzed using inverse gas chromatography (iGC) (Table S1). CNF/2.5CS was found to have a higher surface energy, 62.8 mJ/$m^2$, than neat CNF, 53.4 mJ/$m^2$. These results indicate that the surface of the CS-modified sample is more heterogenous, especially in relation to the acid-based (polar) component, likely due to the presence of amine groups on the CS surface. The crystallinity of the CNF, measured using solid state nuclear magnetic resonance spectroscopy (ssNMR), also increased slightly after functionalization, increasing from 46.5% in CNF to 47.2% in the CNF/2.5CS sample. This slight difference in crystallinity could indicate a minor change in the sample composition but is too close to draw any significant conclusion. These combined characterization results confirmed that spray dried CNF was successfully functionalized with CS.

After confirming the CS functionalization of CNF, initial studies were performed to determine the optimal loading of CS in a PLA composite. Different fiber compositions (CNF, CNF/2.5CS, CNF/5CS, and CNF/7.5CS) were melt compounded with PLA at a 5 wt% total fiber content. During melt compounding, the shear forces and heat can theoretically lead to a reaction between the CS amine groups and PLA acid chain-ends to produce amide bonds. However, due to the low overall CS loading in these composites, the formation of an amide bond cannot be confirmed and is therefore only speculative. This supposed covalent bonding combines with strong hydrogen bonding among the PLA, CS, and CNF to produce a dual bond-strengthened interfacial phase between the filler and the matrix (Fig. 3). Composites featuring CNF/2.5CS marginally displayed the best mechanical properties, which is a similar optimal loading to

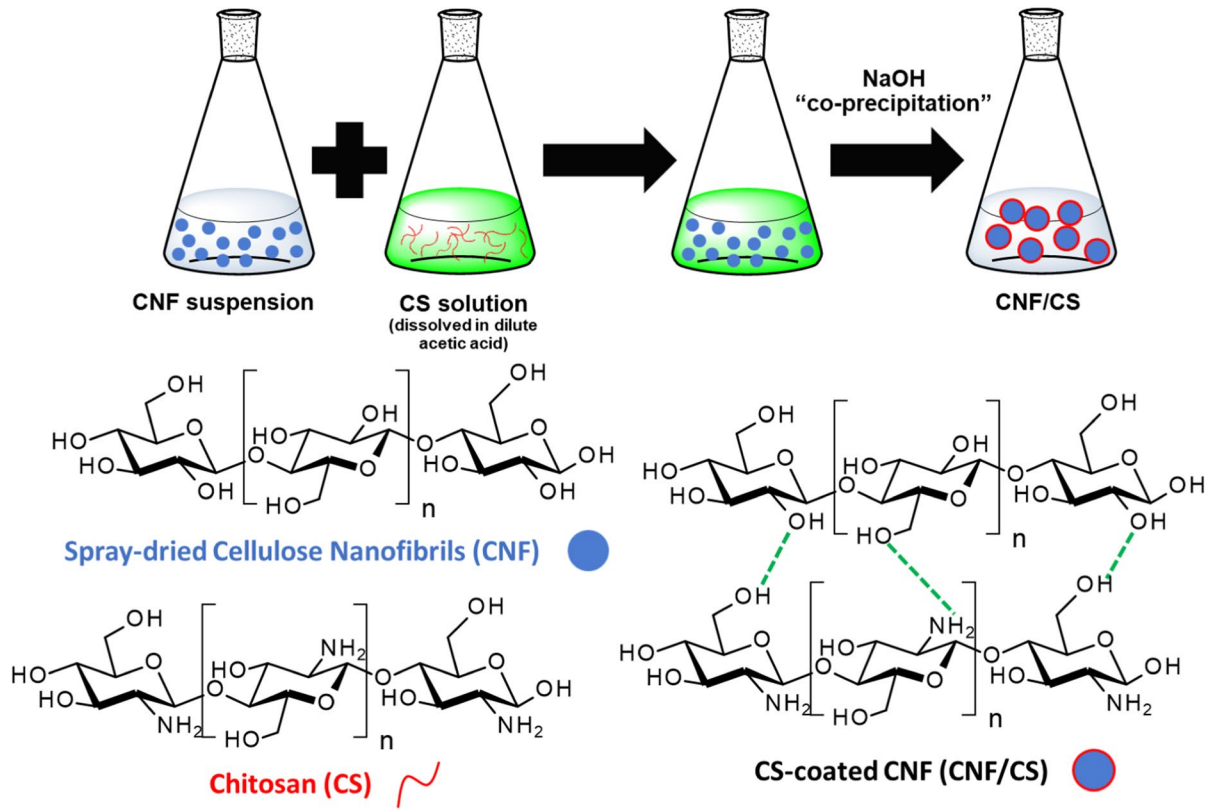


**Scheme 1** Synthesis of CS functionalized CNF (CNF/CS) using a co-precipitation strategy

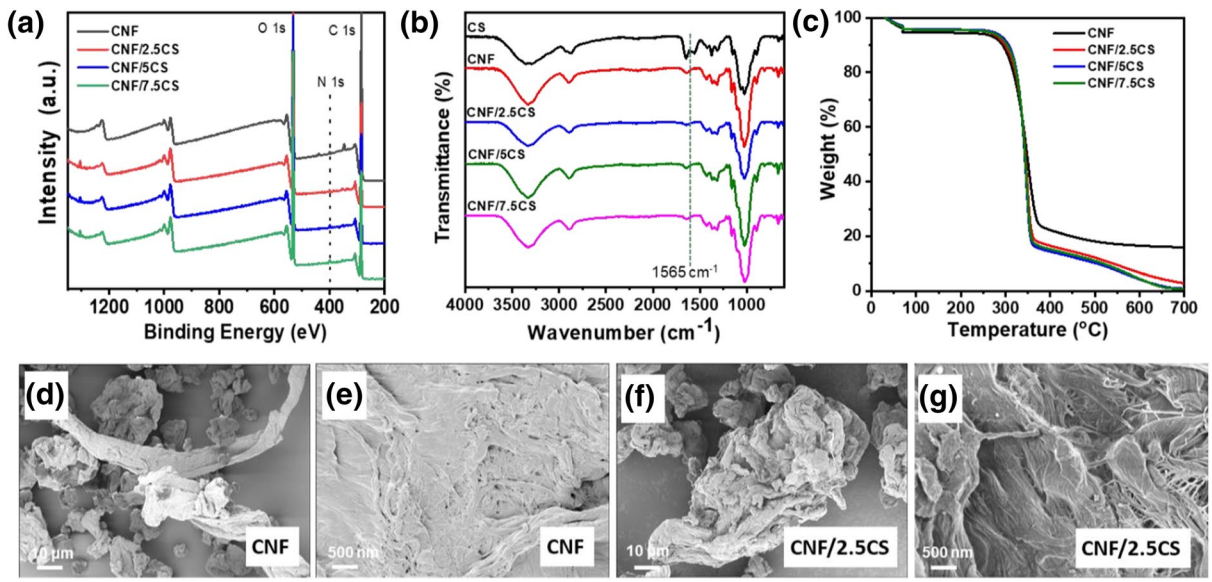


**Fig. 1** Characterization of synthesized CS-CNF. (**a**) XPS Spectra, (**b**) FTIR spectra, **c**) thermal degradation measured using TGA, and morphological characterization using SEM of (**d/e**) CNF, and (**f/g**) CNF/2.5CS

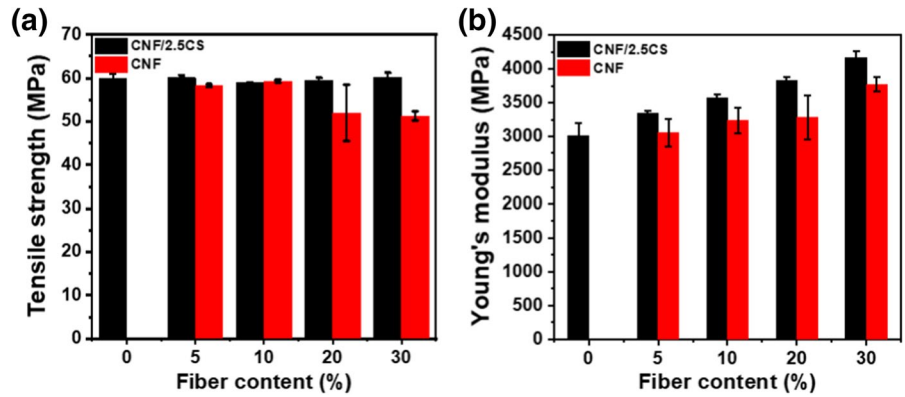


**Fig. 2** Tensile properties of PLA + CNF/CS composites featuring CNF/2.5CS at varying overall fiber contents including, (**a**) Tensile strength and (**b**) Young's modulus

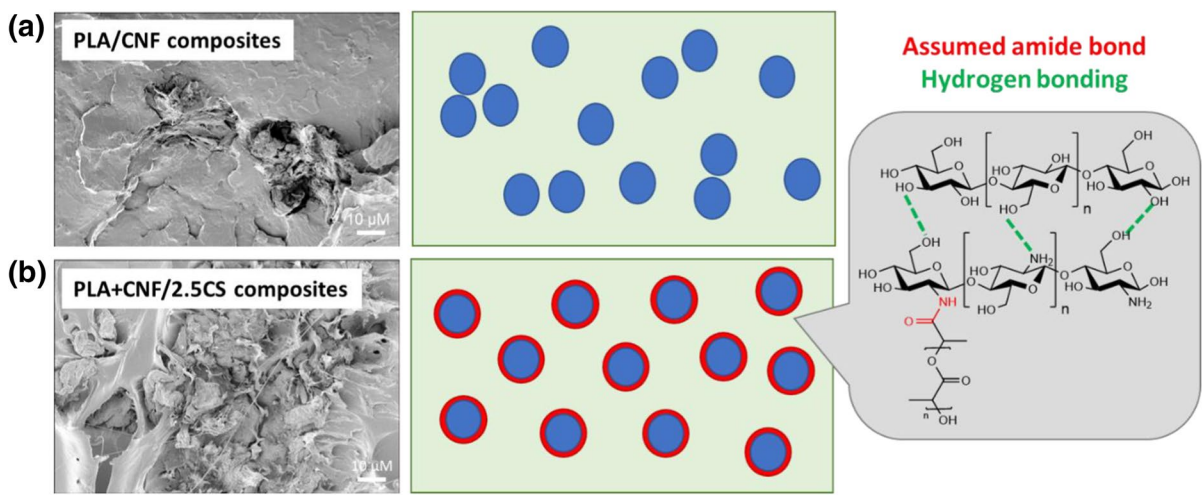


**Fig. 3** SEM images and schematic drawing explaining the interface and dispersion differences between CNF fibers and PLA matrix for (**a**) unmodified CNF and (**b**) functionalized CNF/CS, red indicating the potential amide bond formation

others in literature (Fig. S2) (Shah et al. 2008). Additionally, higher loadings of CS resulted in debonding between the filler and the matrix, which could be observed on SEM images where direct delamination between the CS and PLA is present in the PLA + 5%CNF/7.5CS sample (Fig. S3). In the higher CS content samples, a CS majority phase develops at the interface, delaminates, and cannot properly dissipate mechanical stress, resulting in premature failure. This has been observed in literature, where an increasing the CS loading from 2 to 10 wt% produced morphology issues and resulted in a drastic loss in tensile strength (Kamaludin et al. 2021).

PLA + CNF/CS composites

After the level of CS coated on the CNF surface was optimized at 2.5 wt%, the overall fiber content in composites was explored. A range of PLA + CNF and PLA + CNF/2.5CS composites featuring 5–30 wt.% modified and unmodified CNF fiber content was prepared using melt compounding. The tensile testing results of these compositions are given in Fig. 2, with complete details in Table S2. The functionalized CNF/2.5CS composite properties were compared to those of the unmodified CNF composites. All PLA + CNF/2.5CS composites displayed an almost equivalent tensile strength, around 58 MPa,

regardless of filler content, which is similar to unfilled neat PLA. The unmodified samples showed a sharp decrease to about 51 MPa at filler content of 20 wt% and above. The Young's modulus varied greatly with filler. Both types of PLA composites displayed an increase in Young's modulus with increasing filler content. However, the PLA + CNF/2.5CS composite samples had a much higher increase in modulus than their unmodified counterparts, ranging from 3335 to 4166 MPa for CS-containing samples versus 3053–3770 MPa for unmodified CNF samples. A similar increase in modulus with increasing filler content was observed when measuring the storage modulus through dynamic mechanical analysis as well (DMA, Fig. 4b and Table S3). Neat PLA displayed the lowest storage modulus, 2148 MPa, at room temperature (25 °C), while the value of PLA + 30%CNF/2.5CS composite was much higher at 2909 MPa. As this sample contains the highest fiber loading, the reinforcement provided by the fibers produced stiffness that was superior to other samples, as confirmed by both storage modulus and Young's modulus. The strength and modulus are also equal or superior to other modified CNF/PLA composites dried using similarly industrially relevant technology in the literature (Table S4).

These mechanical property results indicated that the interface between filler and matrix is much improved in the modified CNF samples, likely due to the presence of CS and its reinforcing effect. In unmodified CNF composites, despite hydrogen-bonding between the filler and matrix, the difference in hydrophobicity of the matrix and hydrophilicity of the filler creates an unstable interface that debonds with stress and abruptly fails (Figs. 3a and S3D). Meanwhile, the interface in the modified samples is stronger since it theoretically features a dual-bonded interface supported by a stronger covalent amide bond, allowing it to properly dissipate stress (Fig. 3b). The morphology of the modified composites was examined using SEM of the fracture surface and confirmed a strengthened interface (Figure S5). The samples appear homogenous and display an entangled CNF network. Additionally, the fracture surfaces display both PLA and broken CNF fibers. The broken CNF indicates stress was dissipated during testing, supporting the overall proposed mechanism.

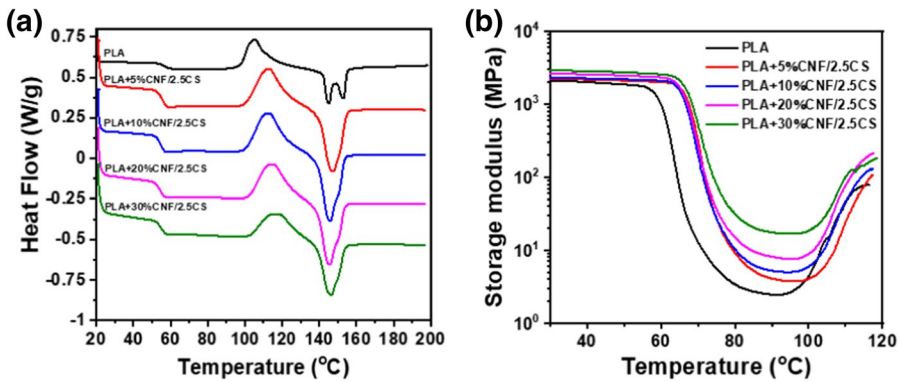


**Fig. 4** Characterization of PLA + CNF/2.5CS composites including (**a**) DSC analysis and (**b**) storage modulus

**Table 2** Thermal properties of the PLA + CNF/2.5CS composites measured using DSC and TGA

| Sample | $T_{5\%}$ (°C) | $T_g$ (°C) | $T_c$ (°C) | $T_m$ (°C) | $\Delta H_c$ (J/g) | $\Delta H_m$ (J/g) | $\chi$ (%) |
|---|---|---|---|---|---|---|---|
| PLA | 325.5 | 56.5 | 105.4 | 145.2, 153.1 | 26.9 | 27.7 | 0.86 |
| PLA + 5%CNF/2.5CS | 327.1 | 55.2 | 100.7 | 147.1 | 20.8 | 25.2 | 4.93 |
| PLA + 10%CNF/2.5CS | 328.3 | 54.5 | 100.8 | 145.6 | 20.9 | 23.2 | 2.71 |
| PLA + 20%CNF/2.5CS | 323.0 | 54.3 | 102.6 | 145.3 | 20.1 | 22.9 | 3.79 |
| PLA + 30%CNF/2.5CS | 319.4 | 54.8 | 103.1 | 146.0 | 14.9 | 18.8 | 6.10 |

$T_{5\%}$: thermal degradation temperature at 5% mass loss. $T_c$: cold crystallization temperature. $T_m$: melting temperature. $\Delta H_c$: enthalpy of crystallization. $\Delta H_m$: enthalpy of melting. $\chi$: degree of crystallization

Thermal properties of the composites were measured using differential scanning calorimetry (DSC) and TGA (Fig. 4a and S6, Table 2). Overall, the onset of thermal degradation of the composites decreased slightly compared to neat PLA (325–318 °C). This is unsurprising given that CNF has lower thermal stability than PLA. While initial addition of filler does increase thermal stability, further increase in the CNF content lowers this degradation temperature. The change in thermal transitions was a bit more complex with variation in filler content. When measured on DSC, the glass transition temperature ($T_g$) stayed fairly constant around 54–56 °C. However, there was a difference when $T_g$ was measured using DMA (Table S3). Using the onset of a drop in storage modulus as an indicator of glass transition, $T_g$ was observed to increase with increasing filler content (59–69 °C at neat PLA and PLA + 30%CNF/2.5CS, respectively). Likewise, a similar trend with $T_g$ was observed when measured using the peak of tan delta (65–73 °C, at neat PLA and PLA + 30%CNF/2.5CS, respectively). This indicates that the filler impedes molecular movement, which is common in composites as the filler physically blocks polymer chains.

The PLA composites underwent cold crystallization during the heating cycle. In neat PLA, the $T_c$ occurred at a slightly higher temperature (105 °C) than the composites (100–103 °C). Crystallization was followed by a melting peak, which displayed a $T_m$ at the same temperature as neat PLA, 145–147 °C. Neat PLA does, however, display two connecting melting points on DSC, which is consistent with our previous studies (Li et al. 2021b). The dual melting peak occurs due to the melting of the different crystal forms/phases present in PLA. The α' form melts at a lower temperature, while the α form melts at the higher one (Pan et al. 2007, 2008). The addition of filler acts as a nucleation site and speeds up the crystallization rate and prevents formation of the α form.

## Conclusions

Surface modification is a proven strategy to alter the hydrophilicity of CNF and aid in its drying and dispersion into polymer matrices. The coprecipitation strategy used in this work successfully produced CS-modified CNFs from commercial spray dried CNF. Initial testing indicated that a CS loading of 2.5 wt% produced the most promising mechanical properties without causing debonding with the PLA matrix. PLA + CNF/2.5CS composites featuring fiber loadings from 5 to 30 wt% were produced using the CNF/2.5CS filler and displayed superior tensile strength and Young's modulus compared to the unmodified spray dried CNF analogues. It is suspected that CS forms a covalent bond with PLA during melt compounding process, complimenting the extensive hydrogen bonding network already present. The results indicated that the dual-bonding system created by the CS modification successfully produces an improved interface between the spray dried CNF fibers and polymer matrix, which could be used as a promising strategy to thrust CNF composites into large-scale, high performance polymer applications.

**Acknowledgments** This research was supported by the U.S. Department of Energy (DOE), Advanced Manufacturing Office and used resources at the Manufacturing Demonstration Facility at Oak Ridge National Laboratory, a User Facility of DOE's Office of Energy Efficiency and Renewable Energy. This manuscript has been authored by UT-Battelle, LLC under Contract No. DE-AC05-00OR22725 with the U.S. Department of Energy. The United States Government retains and the publisher, by accepting the article for publication, acknowledges that the United States Government retains a non-exclusive, paid-up, irrevocable, world-wide license to publish or reproduce the published form of this manuscript, or allow others to do so, for United States Government purposes. The Department of Energy will provide public access to these results of federally sponsored research in accordance with the DOE Public Access Plan (http://energy.gov/downloads/doe-public-access-plan). Microscopy studies were completed at the Center for Nanophase Materials Sciences, a DOE Office of Science User Facility. Authors thank Dr. Harry Meyer for his help on XPS measurement and Dr. Yunqiao Pu for his help on solid state NMR measurement.

**Authors' contribution** MEL: Methodology, Writing—original draft, Writing—review & editing. KL: Conceptualization, Methodology, Software, Writing—review & editing. DK: Investigation. XZ: Investigation, Writing—review & editing. HEH: Investigation. KC: Formal analysis, Writing—review & editing. HT: Writing—review & editing. SO: Writing—review & editing, Supervision, Funding acquisition.

**Funding** This manuscript has been authored by UT-Battelle, LLC under Contract No. DE-AC05-00OR22725 with the U.S. Department of Energy.

**Data availability** The authors confirm that the data supporting the findings of this study are available within the article and its supplementary materials.

**Declarations**

**Conflict of interest** The authors have no relevant financial or non-financial interests to disclose.

## References


Abdul Khalil HPS, Bhat AH, Ireana Yusra AF (2012) Green composites from sustainable cellulose nanofibrils: a review. Carbohydr Polym 87:963–979. https://doi.org/10.1016/j.carbpol.2011.08.078

Abitbol T, Rivkin A, Cao Y, Nevo Y, Abraham E, Ben-Shalom T, Lapidot S, Shoseyov O (2016) Nanocellulose, a tiny fiber with huge applications. Curr Opin Biotechnol 39:76–88. https://doi.org/10.1016/j.copbio.2016.01.002

Abdul Khalil HPS, Saurabh CK, Adnan AS, Nurul Fazita MR, Syakir MI, Davoudpour Y, Rafatullah M, Abdullah CK, Haafiz MKM, Dungani R (2016) A review on chitosan-cellulose blends and nanocellulose reinforced chitosan biocomposites: Properties and their applications. Carbohydr Polym 150:216–226. https://doi.org/10.1016/j.carbpol.2016.05.028

Ali Raza Z, Anwar F, Hussain I, Abid S, Masood R, Shahzad Maqsood H (2019) Fabrication of PLA incorporated chitosan nanoparticles to create enhanced functional properties of cotton fabric. Pigm Resin Technol 48:169–177. https://doi.org/10.1108/PRT-11-2017-0088

An N, Wang X, Li Y, Zhang L, Lu Z, Sun J (2019) Healable and mechanically super-strong polymeric composites derived from hydrogen-bonded polymeric complexes. Adv Mater 31:1904882. https://doi.org/10.1002/adma.201904882

Bakshi PS, Selvakumar D, Kadirvelu K, Kumar NS (2020) Chitosan as an environment friendly biomaterial – a review on recent modifications and applications. Int J Biol Macromol 150:1072–1083. https://doi.org/10.1016/j.ijbiomac.2019.10.113

Beaumont M, König J, Opietnik M, Potthast A, Rosenau T (2017) Drying of a cellulose II gel: effect of physical modification and redispersibility in water. Cellulose 24:1199–1209. https://doi.org/10.1007/s10570-016-1166-9

Bréchet Y, Cavaillé JY, Chabert E, Chazeau L, Dendievel R, Flandin L, Gauthier C (2001) Polymer based nanocomposites: effect of filler-filler and filler-matrix interactions. Adv Eng Mater 3:571–577. https://doi.org/10.1002/1527-2648(200108)3:8%3c571::Aid-adem571%3e3.0.Co;2-m

Cai W, Xue W, Jiang Y (2018) Facile preparation of magnetic chitosan coprecipitated by ethanol/NH3·H2O for highly efficient removal toward Cr(VI). ACS Omega 3:5725–5734. https://doi.org/10.1021/acsomega.8b00393

Conder JR, Young CL (1979) Physicochemical measurement by gas chromatography. John Wiley & Sons

Fowkes FM (1964) Attractive forces at interfaces. Ind Eng Chem 56:40–52. https://doi.org/10.1021/ie50660a008

Fujisawa S, Saito T, Kimura S, Iwata T, Isogai A (2013) Surface engineering of ultrafine cellulose nanofibrils toward polymer nanocomposite materials. Biomacromol 14:1541–1546. https://doi.org/10.1021/bm400178m

Gutmann V (1978) Donor-acceptor approach to molecular interactions. Plenum press

Habibi Y (2014) Key advances in the chemical modification of nanocelluloses. Chem Soc Rev 43:1519–1542. https://doi.org/10.1039/c3cs60204d

Hu X, Vatankhah-Varnoosfaderani M, Zhou J, Li Q, Sheiko SS (2015) Weak hydrogen bonding enables hard, strong, tough, and elastic hydrogels. Adv Mater 27:6899–6905. https://doi.org/10.1002/adma.201503724

Isogai A (2020) Emerging nanocellulose technologies: recent developments. Adv Mater. https://doi.org/10.1002/adma.202000630

Jawaid M, Boufi S, Abdul Khalil HPS (Eds) (2017) Cellulose-reinforced nanofibre composites: production, properties and applications. Woodhead Publishing series in composites science and engineering. Elsevier, Woodhead Publishing, United Kingdom

Kalia S, Boufi S, Celli A, Kango S (2013) Nanofibrillated cellulose: surface modification and potential applications. Coll Polym Sci 292:5–31. https://doi.org/10.1007/s00396-013-3112-9

Kamaludin NHI, Ismail H, Rusli A, Ting SS (2021) Thermal behavior and water absorption kinetics of polylactic acid/chitosan biocomposites. Iran Polym J 30:135–147. https://doi.org/10.1007/s13726-020-00879-5

Lamm ME, Song L, Wang Z, Rahman MA, Lamm B, Fu L, Tang C (2019) Tuning mechanical properties of biobased polymers by supramolecular chain entanglement. Macromolecules 52:8967–8975. https://doi.org/10.1021/acs.macromol.9b01828

Lamm ME, Li K, Qian J, Wang L, Lavoine N, Newman R, Gardner DJ, Li T, Hu L, Ragauskas AJ, Tekinalp H, Kunc V, Ozcan S (2021) Recent advances in functional materials through cellulose nanofiber templating. Adv Mater 33:e2005538. https://doi.org/10.1002/adma.202005538

Li K, Skolrood L, Aytug T, Tekinalp H, Ozcan S (2019) Strong and tough cellulose nanofibrils composite films: mechanism of synergetic effect of hydrogen bonds and ionic interactions. ACS Sustain Chem Eng 7:14341–14346. https://doi.org/10.1021/acssuschemeng.9b03442

Li K, Clarkson CM, Wang L, Liu Y, Lamm M, Pang Z, Zhou Y, Qian J, Tajvidi M, Gardner DJ, Tekinalp H, Hu L, Li T, Ragauskas AJ, Youngblood JP, Ozcan S (2021a) Alignment of cellulose nanofibers: harnessing nanoscale properties to macroscale benefits. ACS Nano 15:3646–3673. https://doi.org/10.1021/acsnano.0c07613

Li K, McGrady D, Zhao X, Ker D, Tekinalp H, He X, Qu J, Aytug T, Cakmak E, Phipps J, Ireland S, Kunc V, Ozcan S (2021b) Surface-modified and oven-dried microfibrillated cellulose reinforced biocomposites: cellulose network enabled high performance. Carbohydr Polym 256:117525. https://doi.org/10.1016/j.carbpol.2020.117525

Liu D, Sun X, Tian H, Maiti S, Ma Z (2013) Effects of cellulose nanofibrils on the structure and properties on PVA nanocomposites. Cellulose 20:2981–2989. https://doi.org/10.1007/s10570-013-0073-6

Lu Y, Cueva MC, Lara-Curzio E, Ozcan S (2015) Improved mechanical properties of polylactide nanocomposites-reinforced with cellulose nanofibrils through interfacial engineering via amine-functionalization. Carbohydr

Polym 131:208–217. https://doi.org/10.1016/j.carbpol.2015.05.047
Meng XT, Bocharova V, Tekinalp H, Cheng SW, Kisliuk A, Sokolov AP, Kunc V, Peter WH, Ozcan S (2018) Toughening of nanocelluose/PLA composites via bio-epoxy interaction: mechanistic study. Mater Design 139:188–197. https://doi.org/10.1016/j.matdes.2017.11.012
Missoum K, Belgacem MN, Bras J (2013) Nanofibrillated cellulose surface modification: a review. Materials (basel) 6:1745–1766. https://doi.org/10.3390/ma6051745
Nechyporchuk O, Belgacem MN, Bras J (2016) Production of cellulose nanofibrils: a review of recent advances. Ind Crops Prod 93:2–25. https://doi.org/10.1016/j.indcrop.2016.02.016
Niu X, Liu Y, Song Y, Han J, Pan H (2018) Rosin modified cellulose nanofiber as a reinforcing and co-antimicrobial agents in polylactic acid /chitosan composite film for food packaging. Carbohydr Polym 183:102–109. https://doi.org/10.1016/j.carbpol.2017.11.079
Pan P, Kai W, Zhu B, Dong T, Inoue Y (2007) Polymorphous crystallization and multiple melting behavior of poly(l-lactide): molecular weight dependence. Macromolecules 40:6898–6905. https://doi.org/10.1021/ma071258d
Pan P, Zhu B, Kai W, Dong T, Inoue Y (2008) Polymorphic transition in disordered poly(l-lactide) crystals induced by annealing at elevated temperatures. Macromolecules 41:4296–4304. https://doi.org/10.1021/ma800343g
Peng YC, Gardner DJ, Han YS (2012) Drying cellulose nanofibrils: in search of a suitable method. Cellulose 19:91–102. https://doi.org/10.1007/s10570-011-9630-z
Peng Y, Gardner DJ, Han Y, Cai Z, Tshabalala MA (2013) Influence of drying method on the surface energy of cellulose nanofibrils determined by inverse gas chromatography. J Coll Interface Sci 405:85–95. https://doi.org/10.1016/j.jcis.2013.05.033
Peng J, Ellingham T, Sabo R, Turng L-S, Clemons CM (2014) Short cellulose nanofibrils as reinforcement in polyvinyl alcohol fiber. Cellulose 21:4287–4298. https://doi.org/10.1007/s10570-014-0411-3
Peresin MS, Habibi Y, Zoppe JO, Pawlak JJ, Rojas OJ (2010) Nanofiber composites of polyvinyl alcohol and cellulose nanocrystals: manufacture and characterization. Biomacromol 11:674–681. https://doi.org/10.1021/bm901254n
Pu S, Hou Y, Yan C, Ma H, Huang H, Shi Q, Mandal S, Diao Z, Chu W (2018) In situ coprecipitation formed highly water-dispersible magnetic chitosan nanopowder for removal of heavy metals and its adsorption mechanism. ACS Sustain Chem Eng 6:16754–16765. https://doi.org/10.1021/acssuschemeng.8b04028
Rinaudo M (2006) Chitin and chitosan: properties and applications. Prog Polym Sci 31:603–632. https://doi.org/10.1016/j.progpolymsci.2006.06.001
Rizal S, Saharudin NI, Olaiya NG, Khalil HPSA, Haafiz MKM, Ikramullah I, Muksin U, Olaiya FG, Abdullah CK, Yahya EB (2021) Functional properties and molecular degradation of schizostachyum brachycladum bamboo cellulose nanofibre in PLA-chitosan bionanocomposites. Molecules 26:2008
Rol F, Belgacem MN, Gandini A, Bras J (2019) Recent advances in surface-modified cellulose nanofibrils. Prog Polym Sci 88:241–264. https://doi.org/10.1016/j.progpolymsci.2018.09.002
Schultz J, Lavielle L, Martin C (1987) The role of the interface in carbon fibre-epoxy composites. J Adhes 23:45–60. https://doi.org/10.1080/00218468708080469
Shah BL, Selke SE, Walters MB, Heiden PA (2008) Effects of wood flour and chitosan on mechanical, chemical, and thermal properties of polylactide. Polym Compos 29:655–663. https://doi.org/10.1002/pc.20415
Sinquefield S, Ciesielski PN, Li K, Gardner DJ, Ozcan S (2020) Nanocellulose dewatering and drying: current state and future perspectives. ACS Sustain Chem Eng 8:9601–9615. https://doi.org/10.1021/acssuschemeng.0c01797
Tekinalp HL, Meng X, Lu Y, Kunc V, Love LJ, Peter WH, Ozcan S (2019) High modulus biocomposites via additive manufacturing: Cellulose nanofibril networks as "microsponges." Compos B Eng. https://doi.org/10.1016/j.compositesb.2019.05.028
Wang L, Gardner DJ, Bousfield DW (2018a) Cellulose nanofibril-reinforced polypropylene composites for material extrusion: rheological properties. Polym Eng Sci 58:793–801. https://doi.org/10.1002/pen.24615
Wang L, Roach AW, Gardner DJ, Han Y (2018b) Mechanisms contributing to mechanical property changes in composites of polypropylene reinforced with spray-dried cellulose nanofibrils. Cellulose 25:439–448. https://doi.org/10.1007/s10570-017-1556-7
Wang L, Gardner DJ, Wang J, Yang Y, Tekinalp HL, Tajvidi M, Li K, Zhao X, Neivandt DJ, Han Y, Ozcan S, Anderson J (2020) Towards industrial-scale production of cellulose nanocomposites using melt processing: a critical review on structure-processing-property relationships. Compos B Eng 201:108297. https://doi.org/10.1016/j.compositesb.2020.108297
Zhao X, Li K, Wang Y, Tekinalp H, Richard A, Webb E, Ozcan S (2020) Bio-treatment of poplar via amino acid for interface control in biocomposites. Compos B Eng 199:108276. https://doi.org/10.1016/j.compositesb.2020.108276
Zhou Y, Fan M, Chen L (2016) Interface and bonding mechanisms of plant fibre composites: an overview. Compos B Eng 101:31–45. https://doi.org/10.1016/j.compositesb.2016.06.055
Zimmermann MVG, Borsoi C, Lavoratti A, Zanini M, Zattera AJ, Santana RMC (2016) Drying techniques applied to cellulose nanofibers. J Reinf Plast Compos 35:628–643. https://doi.org/10.1177/0731684415626286